


# Heat Treatment Effects on Microstructure and Hardness of Low-Carbon AISI 1020 Steel

P. Pavan Kumar Reddy<sup>1</sup> · Saurabh Dewangan<sup>1</sup>  ·  
Rana Sunny Singh<sup>1</sup> · Uttkrishit Singhal<sup>2</sup> ·  
Amrita Biswas<sup>2</sup>

Received: 27 February 2024 / Accepted: 28 March 2024  
© The Institution of Engineers (India) 2024

**Abstract** Heat treatment can change the properties of any metal by changing its size and orientation of grain structure. Structural steel is particularly sensitive to heat treatment. The material's microstructural orientation can change the material's mechanical properties. The current study provides 7 different heat treatment methods that drastically vary cooling rates to allow for detailed microstructural analysis. In order to analyze the microstructural changes in heat-treated samples, one additional sample was kept in "original" or "as received" state. An optical microscope was used to observe the variations in the grain structure. In addition, FESEM (field emission scanning emission microscope) was used to observe the highly magnified images. Using X-ray diffraction (XRD), the crystal structure in each sample was also studied. The stepped cooling procedures (e.g., sand + water, sand + oil) followed in this work are effective in preventing the formation of martensite. Also, a substantial reduction in hardness was achieved after the stepped cooling process done in the sand + water medium.

**Keywords** AISI 1020 · Heat treatment · Cooling rates · Optical microscopy · FESEM · XRD

## Introduction

AISI-1020 grade is a low-carbon steel that is known for its good strength, fair machinability, weldability, and malleability. It is generally manufactured in the form of tubes or square cross-sectional beams which further formed into various products like angles, channels, bars, rods, etc. It possesses a minimum tensile strength of 450 MPa and yield strength of 320 MPa. It can elongate up to 35–40% till fracture. It can be easily cold and hot drawn by using appropriate forming apparatus. These mechanical properties can be greatly modified by applying various heat treatments to them. Low-carbon steel can also be easily quenched and tempered to get a wide range of properties. It is well known that steel gains hardness with an increase in carbon content. On the other side, ductility also gets reduced with increasing carbon amount. Common chemical composition in AISI-1020-0.18% C steel is: carbon (C) = 0.20%; manganese (Mn) = 0.40%; phosphorous (P) ≤ 0.03; sulfur (S) ≤ 0.04 [1, 2]. Heat treating is a thermo-mechanical metal working process that involves heating, holding, and cooling the metal to get the desired physical and chemical characteristics. Heat treatment, sometime, may be used to restore the original properties of the metal. Properties like ductility, toughness, hardness, yield strength, ultimate tensile strength and fracture resistance can be significantly varied by applying different heat treatment techniques. All the heat treatment processes involve a controlled heating and soaking. For the purpose, an adequate size of furnace, heating environment and proper equipment are required. After a certain level of heating, metal is cooled at desired rate- slow, fast, and very

---

✉ Saurabh Dewangan  
saurabh22490@gmail.com

P. Pavan Kumar Reddy  
pavanreddy89789@gmail.com

Rana Sunny Singh  
rana.199402060@mu.j.manipal.edu

Uttkrishit Singhal  
uttkrishit.199402018@mu.j.manipal.edu

Amrita Biswas  
amrita.biswas.chem@gmail.com

<sup>1</sup> Department of Mechanical Engineering, Manipal University Jaipur, Jaipur, Rajasthan 303007, India

<sup>2</sup> Department of Chemistry, Manipal University Jaipur, Jaipur, Rajasthan 303007, India

fast. Three stages of heat treatment are discussed briefly below: (a) Heating stage; (b) Soaking stage; (c) Cooling stage [3, 4]. The objective of the *heating stage* is to heat the metal uniformly in a furnace. In the *soaking stage*, metal is allowed to soak the heat properly so that required phase changes can happen in metal. In the *cooling stage*, the properly heated or soaked metal is ready to cool up to room temperature. For this, various cooling media are used including Air, Water, Oil, Sand, Brine, Furnace, Gas chamber, Powder packed chamber, etc. The rate of cooling decides the final microstructure of the metal [26]. In AISI 1020 steel, two types of microstructures such as pearlite (ferrite and cementite), cementite are usually observed in room temperature. Other microstructure such as martensite, retained austenite, and bainite are also reported based on cooling condition of the steel [5].

- *Ferrite ( $\alpha$ )*: It is a pure form of iron that imparts very less (0.008–0.022%) amount of carbon. Therefore, it is the softest structure in iron-carbon phase diagram.
- *Cementite ( $Fe_3C$ )*: It is the hardest structure in iron-carbon diagram. It possesses 6.67% carbon amount either in the form of globules or any other shape of networks between ferrite grains.
- *Pearlite*: In steel, pearlite is the product of eutectoid reaction at 0.8% carbon content where austenite converts, upon cooling, into two solids- ferrite + cementite. These two solids collectively called pearlite which has an alternate layer of ferrite and cementite. This mixture contains 87.5% ferrite and 12.5% cementite.

A considerable variation in hardness and grain structure of three types of steels, such as AISI 1020, 1040, and 1060, were analyzed according to varying cooling rates. Hardness was found to increase with an increment in cooling rate [6]. In a work, AISI D2 steel, i.e., tool steel, was considered under heat treatment so that dimensional stability of the tool can be maintained during machining work. In this work, steel was undergone into a quick-freezing treatment at a temperature range of  $-120$  to  $-150$  °C. As soon as the temperature was reduced, satisfactory dimensional accuracies were being obtained. Also, the best result was noted at a temperature level of  $-150$  °C [7]. Spring steels were subjected to oil-cooling and tempering works to enhance the performance. Steel was first heated to a range of 870 °C, soaked properly and then cooled in oil. In addition, the cooled samples again subjected to annealing process at a temperature range of 450–550 °C. There was huge difference in microstructure reported in the study before and after the annealing work. The martensite and retained austenite formed prior to annealing got fully converted into bainite after annealing. As result of increasing annealing temperature and time, hardness and tear strength got decreased [8]. Die steel was

considered for increasing wear resistance properties after heat treatment. Wear resistance was found in good correlation with austenitizing temperature. Wear resistance got increased when temperature raised from 920 to 1120 °C. As soon as the upper temperature crossed beyond 1220 °C, a decrease in wear resistance was reported. In addition, bainite was found as superior to bainite + martensite mixture [9]. A case study on AISI 1020 steel revealed that ductility and toughness greatly depend upon ferritic microstructure. After treating by annealing, hardening, and normalizing, it was seen that the lowest hardness was mainly found in annealed sample which had mainly ferrite in excess amount [10]. The cooling rate had a high impact on tensile strength. In a work, the low-carbon steel showed the highest hardness for salt-water quenched product and the lowest for annealed sample, although there was a considerable increment in toughness of annealed samples [11]. Another grade of mild steel was found possessing high tensile strength when it was quenched after austenitization [12]. Classified under AISI 1015 category, EN 9 steel was analyzed in pre- and post-heat-treated conditions. A considerable increment in hardness was observed in age-hardened samples. The annealed samples showed a good elongation till fracture. The impact strength of normalized samples was found superior to hardened samples [13]. The cast iron with high chromium content was analyzed for mechanical characteristics and microstructural variation after tempering. Generally, the high chromium cast iron contains carbides (like  $M_7C_3$  and  $M_{23}C_6$ ), martensitic structure and retained austenite. It was seen that  $M_{23}C_6$  got converted into  $M_7C_3$  after heating the sample at austenite range, i.e., a temperature level of 1020 °C. Later, it became fully dissolved into austenite. The subsequent quenching had made the sample too hard because of containing  $M_7C_3$  carbides in excess amount. The quenched product was tempered to increase the impact strength and reduce the hardness [14]. In four different types of heat-treatments in AISI 1040, i.e., annealing at 950 °C, stress-relieving at 590 °C, normalizing at 899 °C, and tempering at 316 °C, mainly tensile strength was found to be modified in different ways. Especially, tensile strength was found the highest in annealed sample but with a loss of ductility [15]. AISI 4340 steel was undergone through two step heat treatment process which involves heating the sample at critical temperature for 2 h and then allowing it for isothermal transformation in a salt bath (mixed with sodium nitrate) followed by air cooling up to room temperature. As a result, the final microstructure comes out as a mixture of ferrite and bainite. With reducing the isothermal holding time, the microstructural constituents had changed to a combination of ferrite and martensite. The second method with a lesser isothermal holding time gave a stiffer product than that of first method [16]. The effect of double hardening process had resulted in a reduction of carbon amount and formation of long and

brittle carbide layers. The results were thoroughly studied by electron backscattered diffraction (EBSD) technique [17]. The properties of H13-tool steel were analyzed under three different experimental conditions, i.e., post-tempering, during-tempering, and during-quenching. During quenching, martensite along with retained austenite was reported. The tempering has removed retained austenite from the sample and restored toughness with a loss of hardness [18]. Many research works indicate the importance of heat treatment in welded joints to remove residual stress generated due to high thermal gradient [19–25]. In recent studies it has been studied how the interlamellar spacing between pearlites affects their proof strength. The ferrite of interstitial free iron has a higher yield compared to the ferrite of pearlite at a similar length scale [27]. A work highlights the role of substructural parameters such as martensite lath, grain size, grain boundary chemistry in defining fracture toughness for high-strength iron-based materials [28]. The development of ultra-high-strength microalloyed steel is discussed in a work. This is a bainite-martensite alloy that is strong and ductile. It is useful for automotive and structural application [29, 30]. A new high-strength steel has been produced using thermomagnetic controlled processing & air cooling after finalizing rolling at 750 °C. One step Q&P was carried out at a temperature of 345 °C below MS (365 °C) followed by a 30 °C partial austenitization at 800 °C followed by a fully austenitized at 930 °C. The combination of ferrite and lathy microstructure is an ideal combination for a low yield ratio [31]. In a similar manner, steel was subjected to a thermally controlled processing process with the finishing rolling temperature at 850 °C and then air-cooled. The resulting microstructure achieved through this process was highly suitable for obtaining a good balance of mechanical characteristics in the steel [32, 33]. In addition, the advanced high-strength steel (QP steel) [34] and ultra-fast heated steel [35] were also taken under partitioning heat treatment for making them mechanical sound. Some studies include coating on the steel surface to make it corrosion protected [36, 37]. AISI steels

are nowadays considered for friction stir welding (FSW) with aluminum plates. The FSW is known as one of the convenient solid-state welding processes [38–40]. As discussed above in literature review section, AISI 1020 grade has been widely investigated to increase its demand for various applications. Research works are still being conducted on AISI-1020, especially in the direction of property enhancement through heat treatment, to explore a new development in metallography of low-carbon steel. In the area of heat treatment, the present work deals with critical characterization of microstructure after applying seven different cooling rates to the samples. One sample (i.e., eighth sample) was kept in as received condition so that a comparative assessment can be done with regard to it. XRD was utilized to study the phases in different samples.

## Experimental Details

The experimental part involves the collection of AISI 1020-low-C steel samples. The elemental composition of this steel has been done on ‘energy-dispersive spectroscopy’. Figure 1 shows the EDS spectra of the steel sample considered under study.

Total 8 such plates were taken under study out of which 7 plates were considered for heat treatment and 1 was kept in original condition. The seven plates were heated up to 900 °C for 1.5 h in an induction furnace. After that, samples were cooled through various cooling media like air, water, sand, oil, sand + water, sand + oil, and furnace. First sample was cooled in atmospheric air which took approximately 2.5 h to get cooled until room temperature. Second sample was cooled by dipping it inside water. The sample gets cooled in 1 min. Third sample was inserted beneath the sand, which is a poor conductor of heat, hence it has provided slow cooling rate, and the sample took nearly 5.5 h to get cooled up to room temperature. Fourth sample was dipped in 1 L mustard oil and the cooling happened after 20 min. Fifth

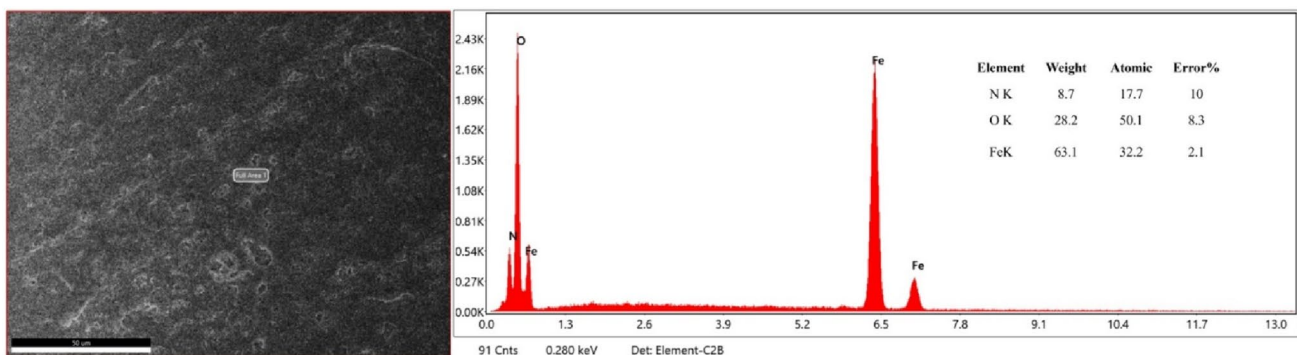
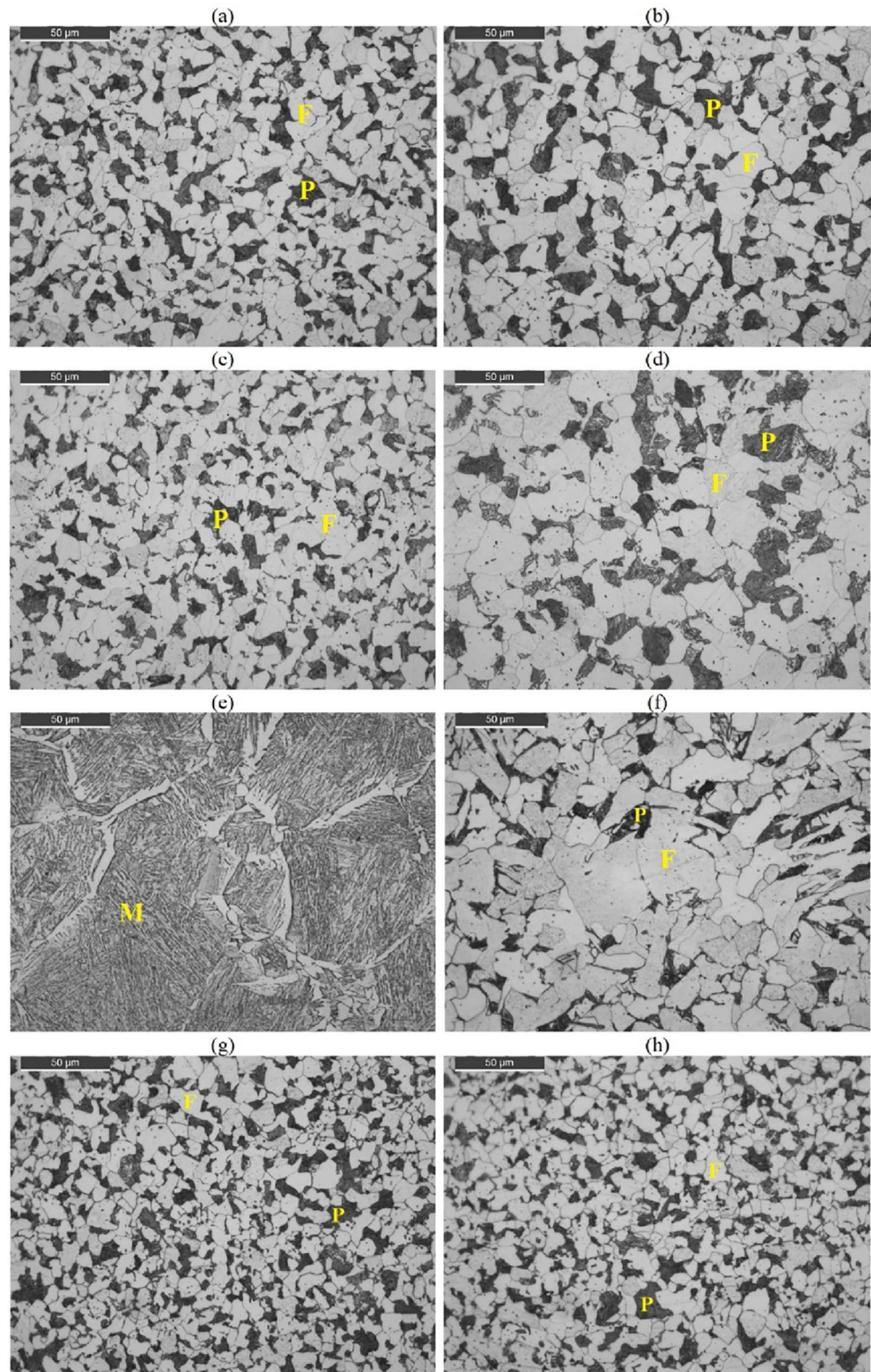


**Fig. 1** EDS spectrum of AISI 1020 steel showing different elements



**Fig. 2** Optical microscopic images at 500 $\times$  magnification and 50  $\mu\text{m}$  scale: F=ferrite; P=pearlite; M = martensite



sample was cooled in two steps- 2 min in sand and then in water till room temperature. In this case, the sample took 4 min to cool down. Similarly, sixth sample was also cooled in two steps- 2 min in sand and then in oil till final cooling. In this case, a total cooling time of 8 min was observed.

The last, seventh sample, one was left in the furnace itself. The power supply of furnace was turned off and the furnace was properly closed so that sample could be isolated from atmosphere. In this case, sample gets cooled down in 40 h. Hence, the cooling media like air, furnace, sand, oil, water,



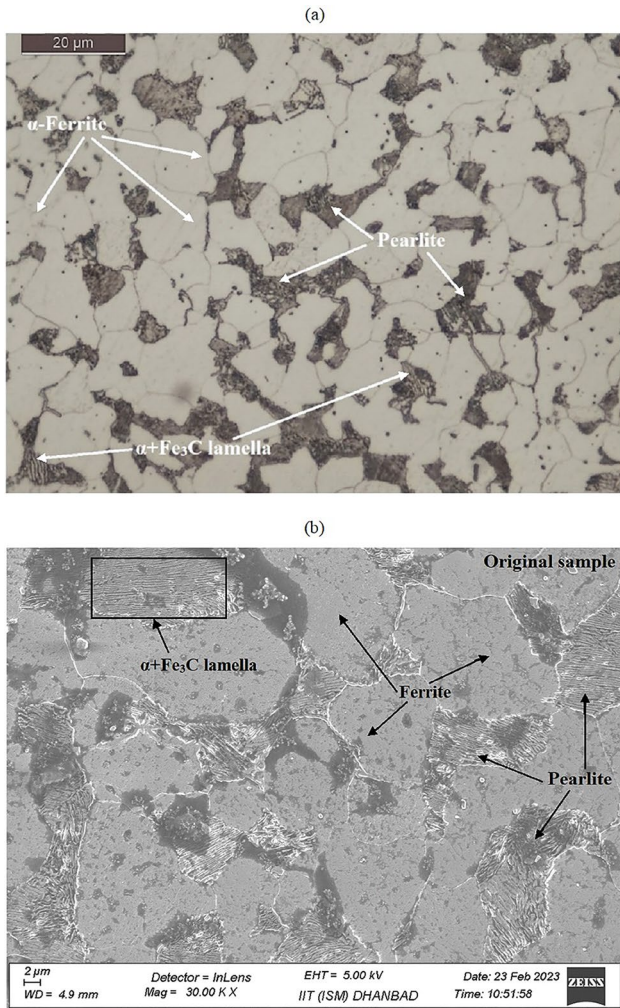


**Fig. 3** Microstructural image of original sample: **a** by OM, **b** by FESEM

sand + oil and sand + water have provided the cooling rates of 0.096 °C/s, 0.006 °C/s, 0.044 °C/s, 0.725 °C/s, 14.5 °C/s, 1.812 °C/s, and 3.625 °C/s, respectively.

The appropriate shaped samples were prepared for microstructural analysis after heat treatment. One side of all the 8 samples were polished by using superfiniting machine. For the purpose, different grades of polishing papers (such as grit sizes of 1000, 1500, 1800, 2200 and 2500) were used in the study. The polishing procedure is indicated in Fig. 2d. Nital (2% nitric acid + 98% ethanol) was applied on the polished surface of samples. An optical microscope with 1000X magnification limit was considered for microstructural observation. In addition, each sample was analyzed under X-ray diffractometer so that phases can be recognized in each sample. Other sides of each sample were utilized for

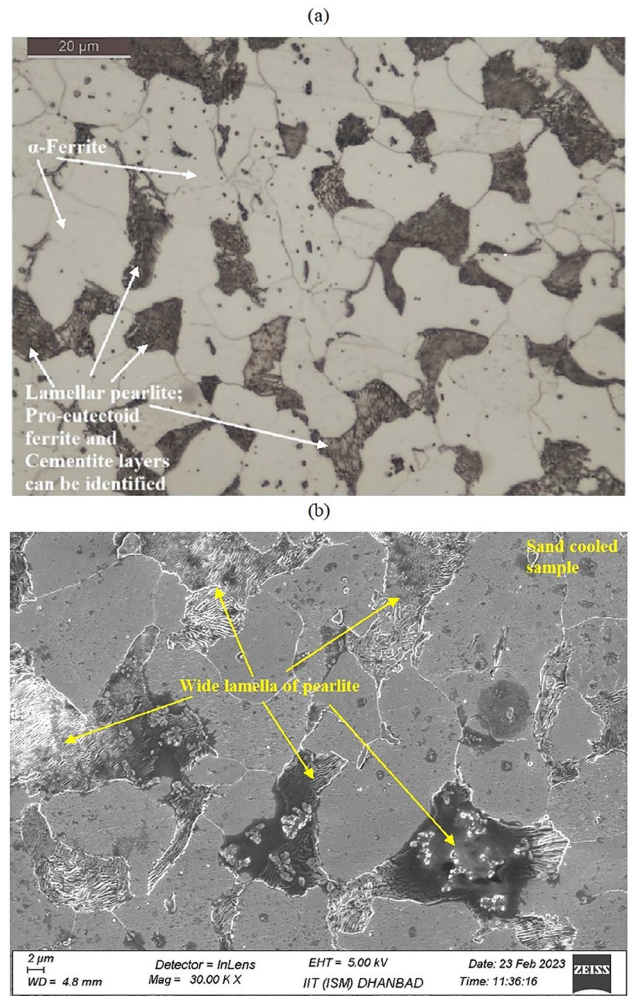


**Fig. 4** Microstructural image of sand-cooled sample: **a** by OM, **b** by FESEM

hardness testing, i.e., indentation through Rockwell hardness test.

### Microstructural Observations and Analysis

The microstructural images were captured by an optical microscope (OM) and FESEM. In OM, the images were captured at two different magnifications 500× and 1000×. For getting the clarity of grain orientation, eight images at 500× magnification are shown in Fig. 2 collectively. For proper comparative analysis, the images captured at 1000× were utilized in the following sections. Similarly, the FESEM images were captured at 30,000× magnification and 2 µm scale. The pearlite lamella was clearly visible through FESEM images. Sample-wise discussion has been provided in the below section:

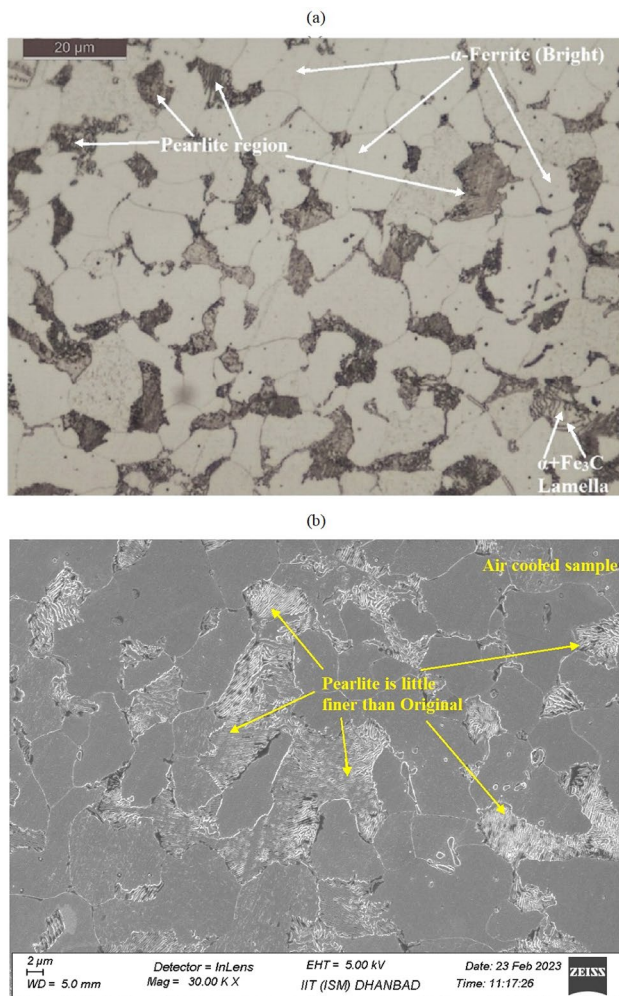


**Fig. 5** Microstructural image of air-cooled sample: **a** by OM, **b** by FESEM

### Original Sample

Initially, the original sample was observed through a microscope. The result of the same was considered as standard for the given type of steel. Figure 3a shows the grain structures of the original sample which consists mainly of  $\alpha$ -ferrite (bright in appearance) and pearlite (Dark in appearance). Some of the pearlitic zones are very dark which resembles that there is very less or no gap between lamella between the  $\alpha$  and  $\text{Fe}_3\text{C}$  (cementite) phases. Also, some widely spaced  $\alpha$  and  $\text{Fe}_3\text{C}$  lamella were observed in this sample by FESEM (Fig. 3b).

### Sand-Cooled Sample

Sand cooling has made the significant changes in microstructural appearance of the steel. As compared to original sample, sand-cooled sample possessed  $\alpha$ -ferrite in wider

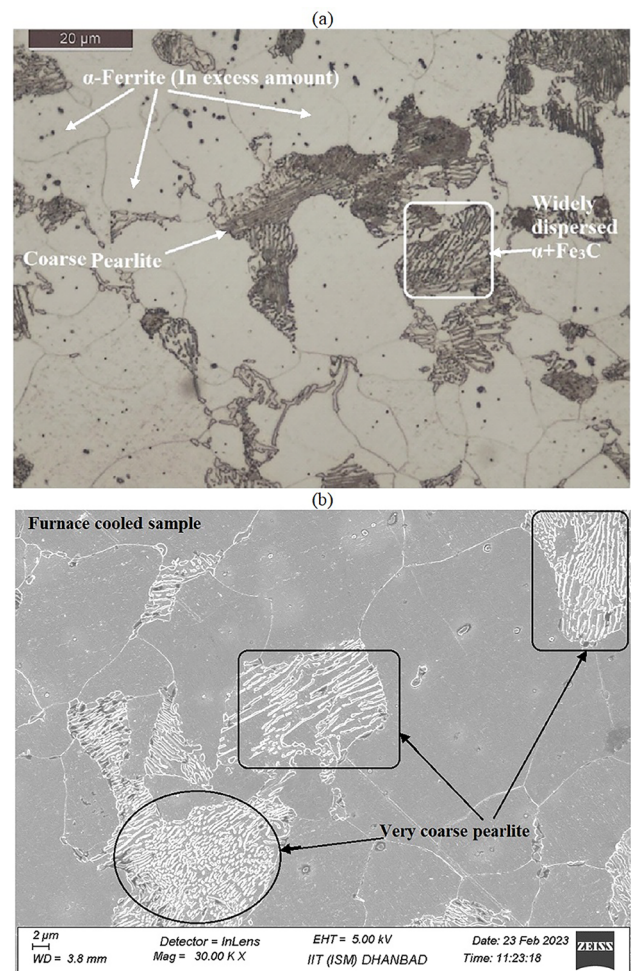


**Fig. 6** Microstructural image of furnace-cooled sample: **a** by OM, **b** by FESEM

area with coarser grain size. The pearlite has mostly lamellar appearance of  $\alpha$ -ferrite and cementite with wider area of dispersion over bright  $\alpha$  zone. The precipitation of cementite over ferrite is more wider than original sample. Wide  $\alpha + \text{Fe}_3\text{C}$  layers can be seen by FESEM (Fig. 4).

### Air-Cooled Sample

Air cooling provides a faster cooling rate than sand cooling. This has converted the coarse grain into finer sizes. The appearance of pearlite is relatively finer than that of original sample and sand-cooled sample. There is very little amount of lamellar  $\alpha + \text{Fe}_3\text{C}$  structure were seen in the image (Fig. 5).

### Furnace-Cooled Sample

In the microscopic image of furnace-cooled sample, a significant variation in both ferrite and pearlite phases was



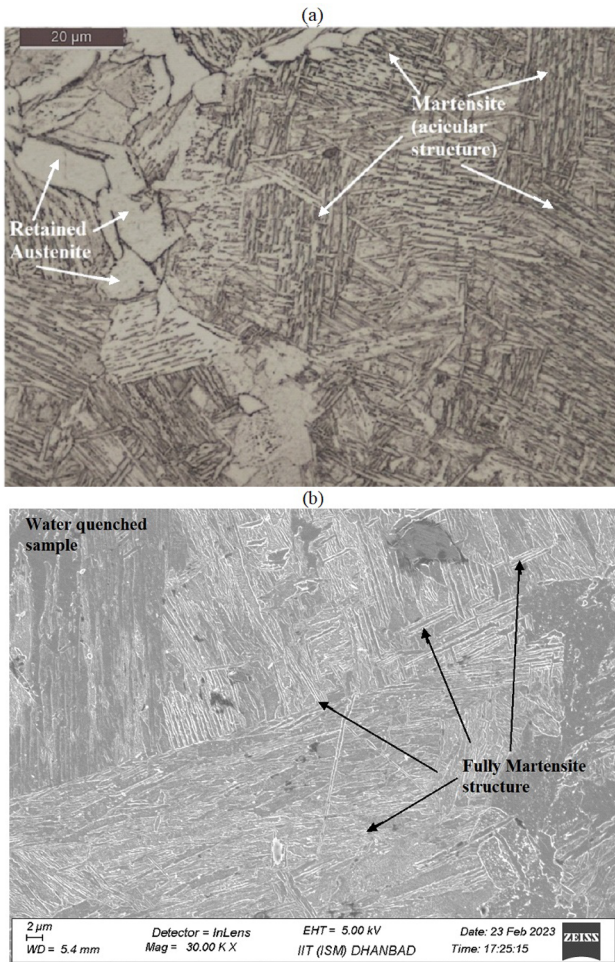


**Fig. 7** Microstructural image of water-cooled sample: **a** by OM, **b** by FESEM

observed (Fig. 6a). In all the pearlitic zones, a widely dispersed  $\alpha + \text{Fe}_3\text{C}$  lamella were noted which means the furnace cooling has made the grain size considerably coarser than that of original sample (Fig. 6).

#### Water-Cooled Sample

The cooling rate provided by water was too fast, and it hardly took 1 min to let the sample cool up to room temperature. At this fast-cooling rate, the  $\gamma$ -austenite (probably formed at 900 °C) has not fully transformed into pearlite. The microstructure mainly consists of acicular needle-like appearance, called martensite. Along with these, the plates-like appearance was also noted in the same which resembles as  $\alpha$ -ferrite, although its presence is low (Fig. 7).

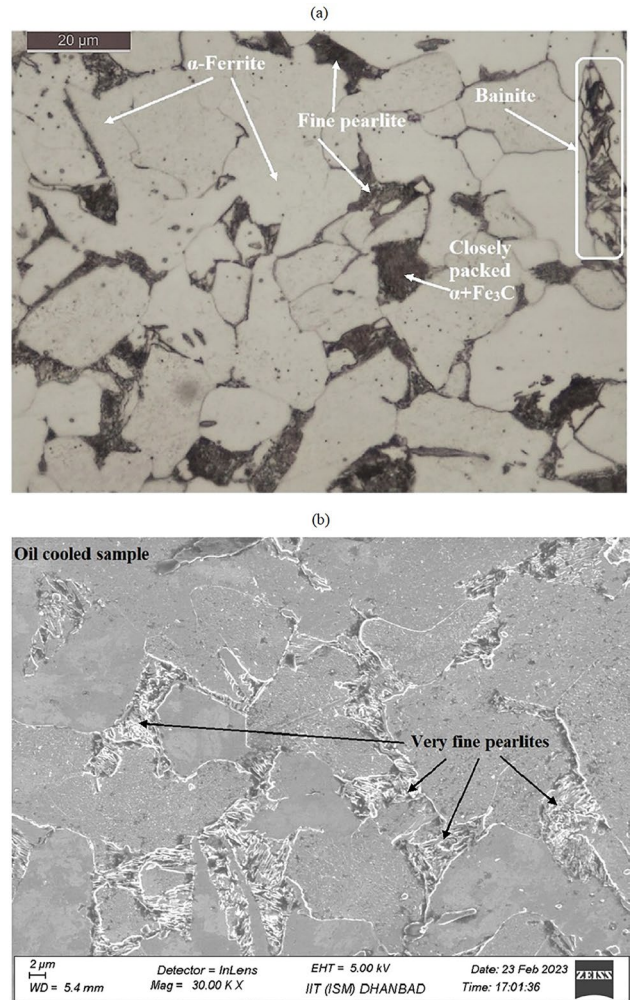


**Fig. 8** Microstructural image of oil-cooled sample: **a** by OM, **b** by FESEM

#### Oil-Cooled Sample

Oil also provides a fast-cooling rate but a little slower than water. Unlike water-cooled sample, it possesses a combination of ferrite, pearlite, and a little amount of bainite. The presence of  $\alpha$ -ferrite is predominant in the image. The pearlite is very fine. No lamellar structure of  $\alpha$  and  $\text{Fe}_3\text{C}$  could be observed in the image. Bainite is a result of fast cooling process. Bainite has also acicular appearance. A very less amount of bainite has been reported in the sample (Fig. 8).

#### Sand + Water-Cooled Sample

As this sample was first buried inside the sand for 2 min, a sufficient time was achieved to transform  $\gamma$ -austenite



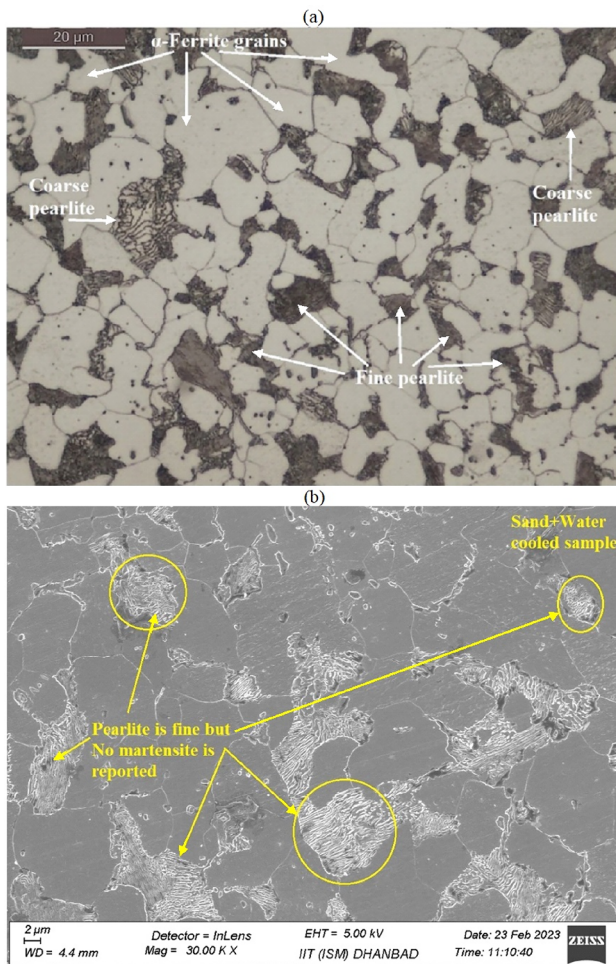


**Fig. 9** Microstructural image of sand+water-cooled sample: **a** by OM, **b** by FESEM

into  $\alpha + \text{Fe}_3\text{C}$ . The subsequent cooling in water resulted in the formation of fine pearlite. Unlike water quenched sample, there is no martensite was reported in this sample. A proper combination of coarse and fine pearlite was achieved in this method. This method is superior than tempering of martensite because a significant changes in microstructure could be done with considerably less energy consumption. At various parts of the sample,  $\alpha + \text{Fe}_3\text{C}$  lamella were reported which is a sign of good ductility and high toughness (Fig. 9).

#### Sand + Oil-Cooled Sample

The attributes of microstructural appearance in this case is similar to sand + water cooling method. It also imparts a clear view of ferrite and pearlite (both fine and coarse), though no sign of bainite formation was reported in this

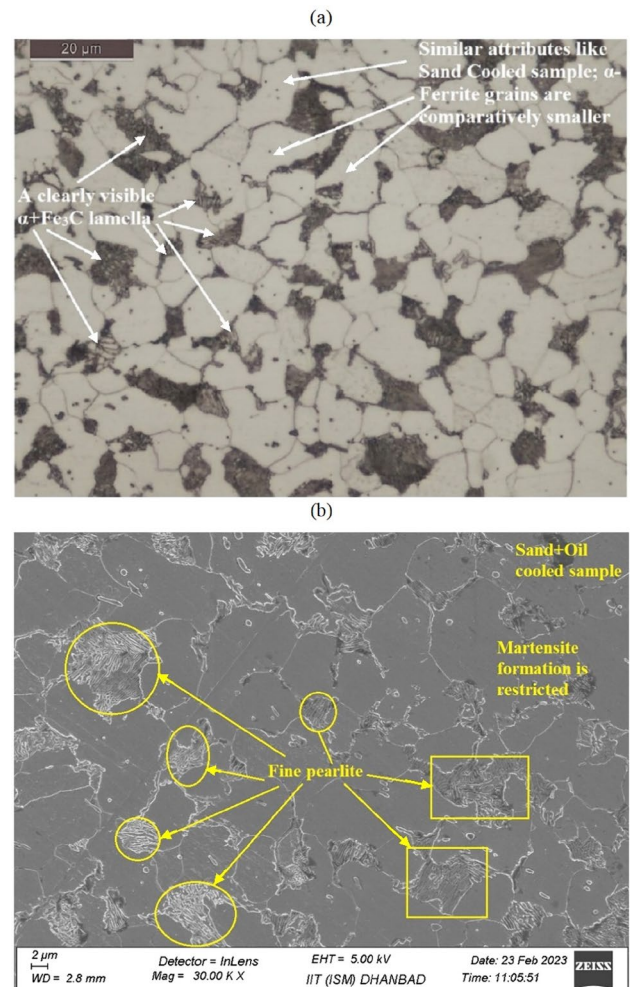


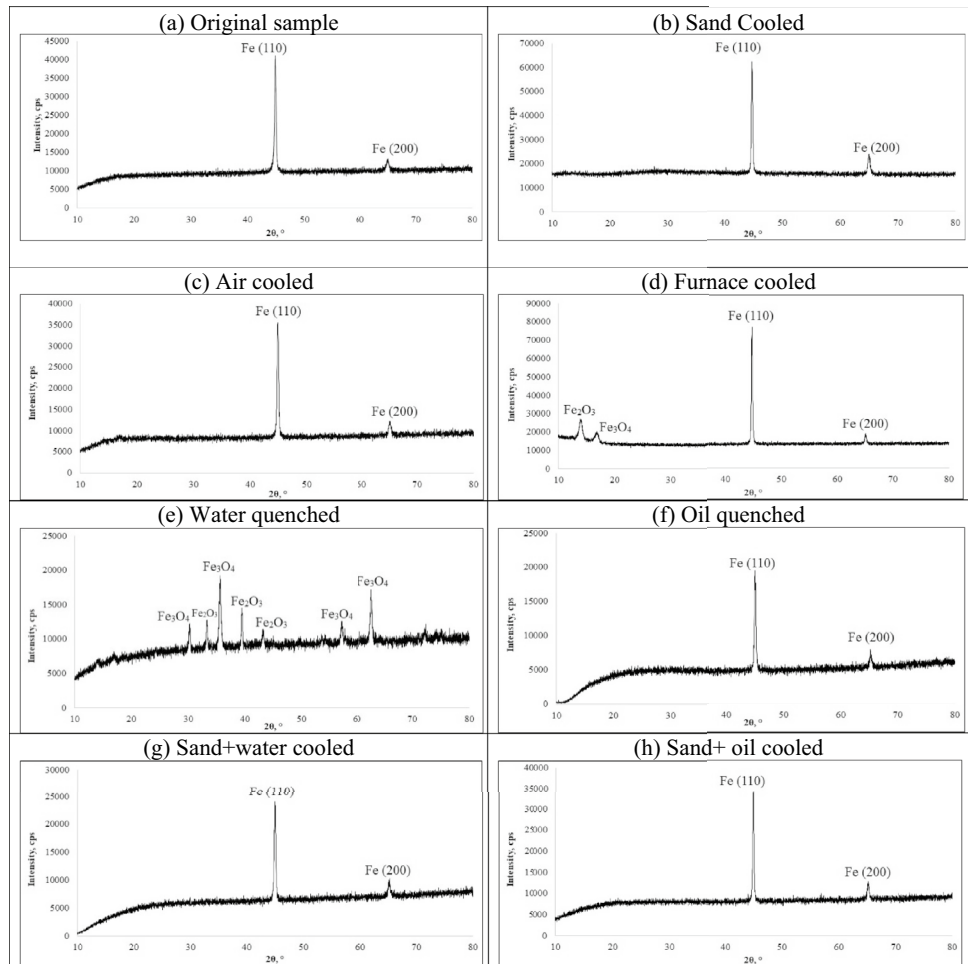
**Fig. 10** Microstructural image of sand+oil-cooled sample: **a** by OM, **b** by FESEM

case. The only difference between plain oil cooling and sand + oil cooling is that the former can give bainite as final microstructure, but latter cannot. The microstructure images are shown in Fig. 10a and b.

#### XRD Analysis

The XRD result of the original sample shows mainly two planes of  $\alpha$ -iron indicated by two different peaks, i.e., a significantly large intensity of plane [110] and comparatively smaller intensity of plane [200]. In this case,  $\alpha$ -ferrite [110] has an intensity of 41,183.334 CPS (Fig. 11a). The sand-cooled sample shows the same plane of iron as in original sample. The intensity of  $\alpha$  [110] has increased in the sand-cooled sample. It is 62,300 CPS for this sample which is about 51% higher than that of the original sample. Figure 11b shows the XRD peaks of the sand-cooled sample. In an air-cooled sample, the intensity

**Fig. 11** XRD analysis in eight samples; intensity versus  $2\theta$  peaks were obtained; mainly two peaks, i.e., ferrite and pro-eutectoid ferrite were noted in samples

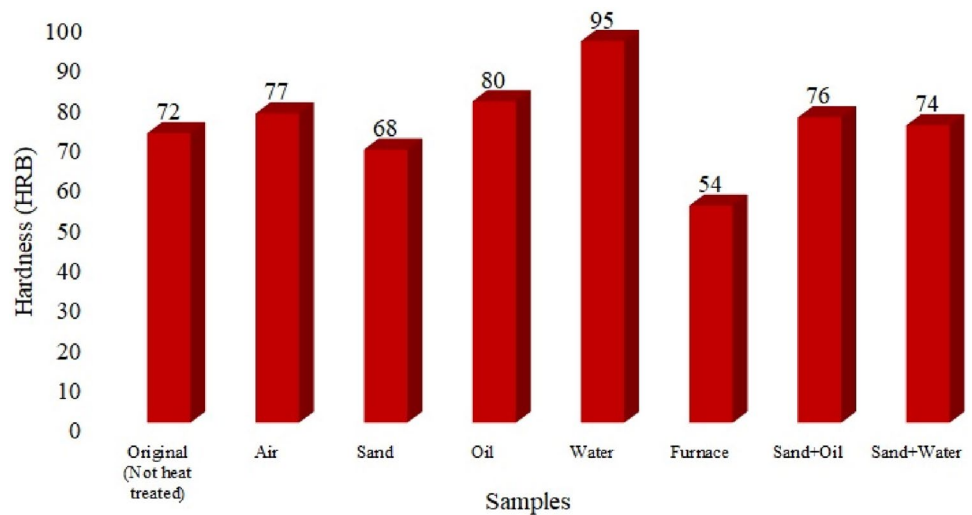


of  $\alpha$ -ferrite (110-plane) is 35,600 CPS. It is nearly 14% lesser than that of the original sample. No other planes that iron were seen in this sample also. The XRD peaks of the air-cooled sample are shown in Fig. 11c. The amount of  $\alpha$ -[110] in the furnace-cooled sample is significantly

higher than that of the original sample. XRD peak of plane [110], in this case, is the highest. The intensity of peak, i.e., 77,416.66 CPS is nearly 88% higher than that of the original sample. Other than pure iron planes, two peaks of iron oxides, named  $Fe_2O_3$  and  $Fe_3O_4$  were also reported at the  $2\theta$  of  $8^\circ$  and  $17^\circ$ , respectively (Fig. 11d). The water quenched sample has shown a complete oxide formation on the metal surface. The  $Fe_3O_4$  peaks were reported at  $2\theta$  of  $30^\circ$ ,  $35^\circ$ ,  $58^\circ$ , and  $63^\circ$  whereas the  $Fe_2O_3$  peaks were visible at the  $2\theta$  of  $32^\circ$ ,  $43^\circ$ , and  $39^\circ$  (Fig. 11e). The results of iron oxide formation are referred from the work of [41–43]. There was no iron oxide formed in the oil quenched sample. The XRD peaks of this sample is similar to that of original sample (Fig. 11f). In sand + water-cooled sample, no proof of iron oxide was reported during XRD analysis. Hence, stepped cooling is useful to avoid the oxide formation along with microstructure restoration (Fig. 11g). The XRD peak of sand + oil-cooled sample revealed a 78% higher intensity of  $\alpha$ -[110] than the same reported in oil-cooled sample (Fig. 11h).

**Table 1** Rockwell hardness measured in HRB

Sr. no	Sample	Hardness in HRB
1	Original	72
2	Air cooled	77
3	Sand cooled	68
4	Oil cooled	80
5	Water cooled	95
6	Furnace cooled	54
7	Sand + oil cooled	76
8	Sand + water cooled	74

**Fig. 12** Comparative analysis among hardness of the samples**Table 2** Overall results outcome of the work

Sample	Microstructure observed	Hardness	
		Values (HRC)	Comparative analysis
Original	Ferrite and pearlite (in normal size)	72	–
Sand cooled	Coarse grains- ferrite and pearlite	68	5%↓
Air cooled	Fine pearlite	77	7%↑
Furnace cooled	Too coarse ferrite and wide lamella of ferrite and cementite	54	25%↓
Water cooled	Martensite and very less ferrite	95	32%↑
Oil cooled	Ferrite, fine pearlite and bainite	80	11%↑
Sand + water-cooled	Ferrite, medium-sized pearlite	74	3%↑
Sand + oil cooled	Ferrite, medium-sized pearlite	76	5%↑

### Hardness Test and Analysis

All the samples were tested through a Rockwell hardness tester to find out the hardness of each sample. A common load value of 150 kgf was applied on each sample through a hardened steel-based indenter. A total of four indents were made on each sample, and an average value of hardness was calculated. The hardness values (HRB) achieved by every sample are given in Table 1. Also, a comparative analysis is provided in Fig. 12.

The overall outcomes of this work can be summarized in Table 2.

The stepped heat treatment provided here, i.e., sand + water and sand + oil cooling processes, can be very useful in industrial applications. A mixture of fine and coarse pearlite was the result of these two treatments. The hardness of the specimens was found higher than those of the

original samples. In addition, the martensite formed because of quenching can be successfully avoided by stepped heat treatment methods. In this way, a lot of energy that is utilized for the tempering of martensite can be saved.

### Conclusion

In this work, an attempt has been made to investigate the microstructural changes and hardness analysis of AISI 0.18%-C steel samples which were heat-treated by 7 different methods. One sample was kept unchanged so that a comparative analysis can be done based on its characteristics. The following observations were made from this work:

- The *original sample*, which was physically unchanged, showed both fine and coarse pearlite along with



$\alpha$ -ferrite phases. The coarse pearlite was in less quantity. XRD peaks showed two planes of iron, i.e., [110] and [200] at  $2\theta$  value of  $44.91^\circ$  and  $65.17^\circ$ , respectively. It possesses a hardness of 72 HRC.

- The microstructure of *air-cooled* sample resembles as of original sample but with finer pearlites. Also, the presence of  $\alpha$ -ferrite got reduced by air cooling.
- A substantial variation in *sand-cooled* sample was seen in the study. A coarse pearlite with lamellar  $\alpha + \text{Fe}_3\text{C}$  has been primarily observed in the sample.
- As a result of very slow cooling, furnace-cooled sample imparts a significant wide lamellar structure of ferrite and cementite. Also, the ferrite grains are too coarse.
- A completely different structure was reported in water-cooled sample which is martensite. Its appearance is needle-like. The iron oxide layers are predominant in this sample, and hence,  $\text{Fe}_2\text{O}_3$  and  $\text{Fe}_3\text{O}_4$  are the two oxides reported in this sample.
- Oil-cooled sample possessed both ferrite and pearlite, yet the lamellar form of pearlite is not visible at all. Unlike water-cooled sample, oil-cooled sample has not showed any oxide formation.
- Sand + water-cooled sample has a completely different microstructure than only water-cooled sample. No martensite was reported, and too some lamellar and coarse pearlite zones were reported along with widely spreaded  $\alpha$ -ferrite. The stepped cooling method has avoided the formation of metal oxide.
- Sand + oil cooling is another option for stepped heat treatment which shows a better improvement in grain structure than in sand + water cooling and only oil cooling.
- Hardness test results are showing the exact characteristics of microstructures in various sample. The order of samples according to hardness is: water-cooled > oil-cooled > air-cooled > sand + oil-cooled > sand + water-cooled > original sample > sand-cooled > furnace-cooled.

**Author Contributions** All the authors contributed to the study, conception, and design. The experimental works were performed by PPKR, RSS and US; AB has done all the result analysis. The compilation of data, and manuscript writing were done by SD. All the authors have read and approved the manuscript before submission.

**Funding** The authors declare that no funds, grants, or other support was received during the preparation of this manuscript.

**Declarations**

**Conflict of interest** The authors have no relevant financial or non-financial interests to disclose.

## References

1. S. Dewangan, N. Mainwal, M. Khandelwal, P.S. Jadhav, Performance analysis of heat treated AISI 1020 steel samples on the basis of various destructive mechanical testing and microstructural behaviour. *Aust. J. Mech. Eng.* **20**(1), 74–87 (2022). <https://doi.org/10.1080/14484846.2019.1664212>
2. S. Dewangan, S. Behera, M.K. Chowrasia, Comparative analysis into mechanical properties and microstructural attributes of quenched and tempered 0.2%-C steel. *World J. Eng.* **17**(1), 127–133 (2020). <https://doi.org/10.1108/WJE-11-2019-0327>
3. S. Dewangan, P. Singhal, S.K. Selvaraj, S.J. Dev, R.S. Swathish, M. Cheepu, S. Legutko, A. Adefris, S. Chattopadhyaya, U. Chadha, Analysing strength, hardness and grain-structure of 0.2%-C steel specimens processed through an identical heating period with different continuous transformation rates. *Mater. Res. Express* (2022). <https://doi.org/10.1088/2053-1591/aca7b2>
4. S. Dewangan, S.K. Selvaraj, B. Karthikeyan, U. Chadha, P. Singhal, P.P. Sarma, P.V. Raju, U. Kumar, M.P. Kumar, Fractography analysis into low-C steel undergone through various destructive mechanical tests. *Mater. Res. Express* (2022). <https://doi.org/10.1088/2053-1591/aca580>
5. W.D. Callister, *An Introduction to Materials Science and Engineering* (John Wiley and Sons Inc, 2007)
6. A. Çalik, Effect of cooling rate on hardness and microstructure of AISI 1020, AISI 1040 and AISI 1060 Steels. *Int. J. Phys. Sci.* **4**(9), 514–518 (2009). <https://doi.org/10.5897/IJPS.9000188>
7. C.H. Surberg, P. Stratton, K. Lingenhole, The effect of some heat treatment parameters on the dimensional stability of AISI D2. *Cryogenics* **48**, 42–47 (2008). <https://doi.org/10.1016/j.cryogenics.2007.10.002>
8. M.S. Htun, S.T. Kyaw, K.T. Lwin, Effect of heat treatment on microstructures and mechanical properties of spring steel. *J. Metals Mater. Miner.* **18**, 191–197 (2008)
9. W. Min-xian, W. Shu-qi, W. Lan, C. Xiang-hong, C. Kang-min, Selection of heat treatment process and wear mechanism of high wear resistant cast hot-forging die steel. *J. Iron. Steel Res. Int.* **19**(5), 50–57 (2012). [https://doi.org/10.1016/S1006-706X\(12\)60099-5](https://doi.org/10.1016/S1006-706X(12)60099-5)
10. S.S. Hossain, M.M. Islam, M.S.A. Bhuyan, A case study of heat treatment on AISI 1020 steel. *Glob. J. Res. Eng. Mech. Mech. Eng.* **14**(5), 35–39 (2014)
11. A.R. George, M. Samson, K. Ottoor, T. Geethapriyan, The effects of heat treatment on the microstructure and mechanical properties of EN19 steel. *Int. J. Mater. Sci. Eng.* **6**(2), 56–66 (2018). <https://doi.org/10.17706/ijmse.2018.6.2.56-66>
12. M.F. Hasan, Analysis of mechanical behavior and microstructural characteristics change of ASTM A-36 steel applying various heat treatment. *J. Material. Sci. Eng.* **5**, 2 (2016). <https://doi.org/10.4172/2169-0022.1000227>
13. U.A. Kini, S.S. Sharma, S.Y. Nayak, S.S. Heckadka, Mechanical characterization of heat treated EN 9 steel. *International Conference on Engineering and Information Technology*, 17–18 (2017), Malaysia, ISBN: 9788193137314 25
14. Z.H. Guo, F. Xiao, S. Lu, H. Li, B. Liao, Effects of heat-treatment on the microstructure and wear resistance of a high-chromium cast iron for rolls. *Adv. Mater. Sci. Eng.* **2016**, 9807685 (2016). <https://doi.org/10.1155/2016/9807685>
15. K.O. Sanusi, E.T. Akinlabi, Experiment on Effect of heat treatment on mechanical and microstructure properties of AISI steel. *Mater. Today Proc.* **5**, 17996–18001 (2018). <https://doi.org/10.1016/j.matpr.2018.06.132>
16. B.M. Gurumurthy, S. Sharma, U.A. Kini, A. Hegde, A. Patil, Mechanical characteristics evaluation of dual phase and related hardening techniques on AISI 4340 steel. *J. Mech. Eng. Sci.* **12**(4),

- 4018–4029 (2018). <https://doi.org/10.15282/jmes.12.4.2018.03.0349>
17. M. Hofinger, M. Staudacher, M. Ognianov, C. Turk, H. Leitner, R. Schnitzer, Microstructural evolution of a dual hardening steel during heat treatment. *Micron* **120**, 48–56 (2019). <https://doi.org/10.1016/j.micron.2019.02.004>
  18. F. Deirmina, N. Peghini, B. AlMangour, D. Grzesiak, M. Pellizzari, Heat treatment and properties of a hot work tool steel fabricated by additive manufacturing. *Mater. Sci. Eng. A* (2019). <https://doi.org/10.1016/j.msea.2019.03.027>
  19. Z. Zhang, H. Zhang, J. Hu, X. Qi, Y. Bian, A. Shen, P. Xu, Y. Zhao, Microstructure evolution and mechanical properties of briefly heat treated SAF 2507 super duplex stainless steel welds. *Constr. Build. Mater.* **168**, 338–345 (2018). <https://doi.org/10.1016/j.conbuildmat.2018.02.143>
  20. A. Järvenpää, M. Jaskari, M. Keskitalo, K. Mäntyjärvi, P. Karjalainen, Microstructure and mechanical properties of laser-welded high-strength AISI 301LN steel in reversion-treated and temper-rolled conditions. *Proc. Manuf.* **36**, 216–223 (2019). <https://doi.org/10.1016/j.promfg.2019.08.028>
  21. A. Sharma, D.K. Verma, S. Kumaran, Effect of post weld heat treatment on microstructure and mechanical properties of Hot Wire GTA welded joints of SA213 T91 steel. *Mater. Today Proc.* **5**, 8049–8056 (2018). <https://doi.org/10.1016/j.matpr.2017.11.490>
  22. S.T. Selvamani, M. Vigneshwara, M. Nikhil, S.J. Hariharan, K. Palanikumar, Enhancing the fatigue properties of friction welded AISI 1020 grade steel joints using post weld heat treatment process in optimized condition. *Mater. Today Proc.* **16**, 1251–1258 (2019). <https://doi.org/10.1016/j.matpr.2019.05.222>
  23. S. Dewangan, S.K. Selvaraj, T.M. Adane, S. Chattopadhyaya, G. Królczyk, R. Raju, Metallographic investigation on postweld heat-treated .021% C-1020 steel plates joined by SMAW method. *Adv. Mater. Sci. Eng.* (2022). <https://doi.org/10.1155/2022/9377591>
  24. S. Dewangan, S. Chattopadhyaya, Analysing effect of quenching and tempering into mechanical properties and microstructure of 304-SS welded plates. *Acta Metall. Slov.* **28**(3), 140–146 (2022). <https://doi.org/10.36547/ams.28.3.1556>
  25. B. Sadeghi, H. Sharifi, M. Rafiei, M. Tayebi, Effects of post weld heat treatment on residual stress and mechanical properties of GTAW: The case of joining A537CL1 pressure vessel steel and A321 austenitic stainless steel. *Eng. Fail. Anal.* **94**, 396–406 (2018). <https://doi.org/10.1016/j.engfailanal.2018.08.007>
  26. A.R. Kulkarni, P.V. Raju, P.P. Sarma, S. Dewangan, S.K. Selvaraj, Microstructure and mechanical properties of 0.18%-C steel samples processed through five different heat treatment techniques. *J. Inst. Eng. India Ser. D* (2024). <https://doi.org/10.1007/s40033-023-00633-0>
  27. H.K.D.H. Bhadeshia, A.R. Chintha, Critical assessment 41: the strength of undeformed pearlite. *Mater. Sci. Technol.* **38**(16), 1291–1299 (2022). <https://doi.org/10.1080/02670836.2022.2079295>
  28. R.D.K. Misra, A perspective in the understanding of strength-toughness combination during processing of engineering ferrous alloys. *Mater. Technol.* (2023). <https://doi.org/10.1080/10667857.2023.2278000>
  29. G. Mandal, S.K. Ghosh, S. Chatterjee, Effects of TMCP and QT on microstructure and properties of ultrahigh strength steel. *Mater. Today Proc.* **18**, 5196–5201 (2019)
  30. G. Mandal, N.K. Tewary, S.K. Ghosh, Enhancement of mechanical properties in bainitic steel processed from different austenitization temperatures. *Steel Res. Int.* **89**(2), 1700259 (2018)
  31. G. Mandal, S.K. Ghosh, S. Bera, S. Mukherjee, Effect of partial and full austenitisation on microstructure and mechanical properties of quenching and partitioning steel. *Mater. Sci. Eng. A* **676**, 56–64 (2016)
  32. G. Mandal, C. Roy, S.K. Ghosh, S. Chatterjee, Structure-property relationship in a 2 GPa grade micro-alloyed ultrahigh strength steel. *J. Alloy. Compd.* **705**, 817–827 (2017)
  33. G. Mandal, I. Dey, S. Mukherjee, S.K. Ghosh, Phase transformation and mechanical properties of ultrahigh strength steels under continuous cooling conditions. *J. Market. Res.* **19**, 628–642 (2022)
  34. M. Carpio, J. Calvo, O. García, J.P. Pedraza, J.M. Cabrera, Heat treatment design for a QP steel: effect of partitioning temperature. *Metals* **11**(7), 1136 (2021)
  35. E.I. Hernandez-Duran, V. Bliznuk, T. Ros-Yanez, R. Iquilio-Abarzua, F.M. Castro-Cerda, R.H. Petrov, Improvement of the strength-ductility balance in ultrafast heated steels by combining high-temperature annealing and quenching and partitioning process. *Mater. Sci. Eng. A* **827**, 142045 (2021)
  36. D. Singh, A. Goyal, A. Saini, S. Sonewane, K.K. Saxena, Vibration and noise analysis of acetoxime modified TiO<sub>2</sub> coating over steel alloy. *Int. J. Interact. Des. Manuf. (IJIDeM)*, 1–9 (2022)
  37. A. Saini, D. Singh, V. Dhayal, Structural and optical properties of titania nanostructures obtained from oxime-modified titanium (IV) precursor. *Mater. Res. Innovations* **26**(5), 276–284 (2022)
  38. R. Kumar, B. Bora, S. Chattopadhyaya, G. Krolczyk, S. Hloch, Experimental and mathematical evaluation of thermal and tensile properties of friction stir welded joint. *Int. J. Mater. Prod. Technol.* **57**(1–3), 204–229 (2018)
  39. R. Kumar, B. Bora, S. Chattopadhyaya, G. and Krolczyk, Critical investigation of mechanical and micro-structural properties of friction stir welded joints of AA-6061 T6. *Academic J. Manuf. Eng.*, **17**(4) (2019)
  40. R. Kumar, S. Chattopadhyaya, A.R. Dixit, B. Bora, M. Zelenak, J. Foldyna, S. Hloch, P. Hlavacek, J. Scucka, J. Klich, L. Sitek, Surface integrity analysis of abrasive water jet-cut surfaces of friction stir welded joints. *Int. J. Adv. Manuf. Technol.* **88**, 1687–1701 (2017)
  41. J.H. Lee, J.G. Yun, S.Y. Kwak, C.Y. Kang, Nucleation and growth of intermetallic compounds formed in boron steel hot-dipped in Al–Ni alloy. *Coatings* **7**(11), 195 (2017)
  42. E.M. Koushika, G. Shanmugavelayutham, P. Saravanan, C. Balasubramanian, Rapid synthesis of nano-magnetite by thermal plasma route and its magnetic properties. *Mater. Manuf. Process.* **33**(15), 1701–1707 (2018)
  43. D.P. Joshi, G. Pant, N. Arora, S. Nainwal, Effect of solvents on morphology, magnetic and dielectric properties of ( $\alpha$ -Fe<sub>2</sub>O<sub>3</sub>@SiO<sub>2</sub>) core-shell nanoparticles. *Heliyon* **3** (2017)

**Publisher's Note** Springer Nature remains neutral with regard to jurisdictional claims in published maps and institutional affiliations.

Springer Nature or its licensor (e.g. a society or other partner) holds exclusive rights to this article under a publishing agreement with the author(s) or other rightsholder(s); author self-archiving of the accepted manuscript version of this article is solely governed by the terms of such publishing agreement and applicable law.